Anchoring Group and Auxiliary Ligand Effects on the Binding of Ruthenium Complexes to Nanocrystalline TiO_2 Photoelectrodes

Kristine Kilså, Elizabeth I. Mayo, Bruce S. Brunschwig,* Harry B. Gray,* Nathan S. Lewis,* and Jay R. Winkler*

Beckman Institute and Division of Chemistry and Chemical Engineering, California Institute of Technology, Pasadena, California 91125, USA

Received: October 6, 2003; In Final Form: April 1, 2004

The thermodynamics and kinetics of binding to nanocrystalline TiO_2 were investigated for five ruthenium complexes that differed structurally in the number of possible anchoring carboxy groups (one, two, four, or six) attached to coordinated bipyridyl ligands and in the number of auxiliary ligands (bipyridine, CN^-, or SCN^-). Diffuse reflectance infrared spectroscopic data indicated that the dyes predominantly bound to TiO_2 in a bridging mode in which the oxygen atoms of an attached carboxy group were bound to separate titanium atoms on the TiO_2 surface. Furthermore, in the dry state, complexes with only one monocarboxy or dicarboxy ligand used essentially all of their available carboxy groups to bind to the surface. However, complexes having two or three dicarboxy ligands used on average two carboxylato groups in binding to TiO_2. The structural differences between the complexes were manifested chemically in that the five dyes yielded similar maximum coverages (>100 nmol cm^{-2}) on nanocrystalline TiO_2 electrodes, but exhibited different binding constants (10^3-10^5 M^{-1}) and different adsorption and desorption kinetics ($3-11$) $\times$ 10^3 M^{-1} h^{-1} and 1−100 h, respectively). The binding constant for the monocarboxy dye was significantly lower than the binding constants for dyes with dicarboxy ligands, correlating primarily with an increase in the desorption rate of the monocarboxy complex. The adsorption rate constants were similar for all of the dyes, suggesting that formation of the first bond to TiO_2 was rate limiting. Binding of the dyes from an ethanolic solution that contained pyridine and pyridinium as an acidic proton activity buffer yielded lower coverages than binding from a nonbuffered ethanol solution, even though the binding constants were up to 100 times greater under buffered conditions. The lower equilibrium dye coverage in buffered ethanol did not correlate with changes in the protonation state of the dyes but rather indicated competition for, and/or deactivation of, TiO_2 active sites in buffered ethanol. The more weakly bound monocarboxy dye displayed the lowest short-circuit current density and open-circuit voltage under simulated solar illumination in a photoelectrochemical cell containing 0.50 M LiI, 0.040 M I_2, 0.020 M pyridine, and 0.020 M pyridinium triflate in acetonitrile. Additionally, even at constant coverage, the integrated quantum yield for photocurrent flow was lowest for TiO_2 sensitized with the monocarboxy dye. The potential required to drive 0.1 mA cm^{-2} of cathodic current density in the dark on dye-sensitized TiO_2 photoelectrodes was least negative for the monocarboxy dye, indicating more facile electron transfer between reduced TiO_2 and the solution redox couple. Hence, in this series of ruthenium carboxy-bipyridyl dyes, the most weakly bound species (i.e., the monocarboxy dye) yielded inferior photoelectrode properties, whereas differences between the dyes that contained at least one dicarboxy ligand resulted primarily from differences in the light absorption and energetic properties of the metal complexes. These observations suggest an important role for the linkage to the TiO_2 surface in achieving temporal stability as well as in tuning both the steady-state quantum yield and the magnitude of the predominant back-reaction rate in dye-sensitized TiO_2-based photoelectrochemical solar cells.

I. Introduction

Dye-sensitized solar cells (DSSCs) were shown in the early 1990s to be a promising energy conversion technology.[1] These DSSCs are based on nanocrystalline TiO_2 that is covered by a dye capable of absorbing sunlight and sensitizing the semiconductor. Upon light absorption, the electronically excited dye injects an electron into TiO_2, resulting in oxidized dye and reduced TiO_2. The electron is collected at the back electrode, usually a glass slide coated with fluorine-doped SnO_2. A redox pair in solution, I^-/I_3^-, reduces the oxidized dye and in turn is reduced to its original state at the counter electrode, completing the electrical circuit in the cell.[2,3] The nanocrystalline morphology of the TiO_2 is crucial to solar cell performance, as the large surface area (~1000-fold greater than that of a single crystal of equal projected area) allows the binding of sufficient dye to absorb most of the incident light.

One of the most popular DSSC dyes, Ru(4,4′-dicarboxylic acid-2,2′-bipyridine)$_2$(NCS)$_2$ (the so-called N3 dye; abbreviated herein as $[Ru(H_2L')_2(NCS)_2]^0$), contains four carboxy groups that can be used for anchoring the dye to the TiO_2 surface.[4] Although organic dyes,[5,6] inorganic dyes based on other metals such as iron[7] and osmium,[8] and other anchoring groups such as

* Corresponding authors. Phone: +1 626 395 6500. Fax: +1 626 449 4159. E-mail: bsb@caltech.edu (B.S.B.); hbgray@caltech.edu (H.B.G.); nslewis@caltech.edu (N.S.L.); winklerj@caltech.edu (J.R.W.).

10.1021/jp0369995 CCC: $27.50
Published on Web 09/11/2004

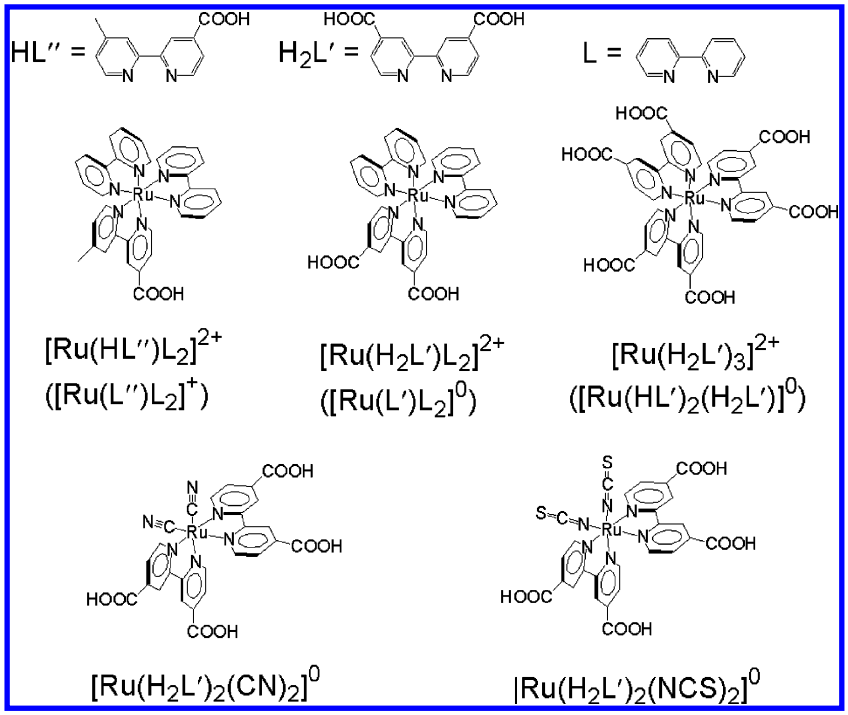

Figure 1. Structures of the fully protonated ligands, HL″, H_2L', and L, and of the fully protonated complexes, $[Ru(HL'')L_2]^{2+}$, $[Ru(H_2L')L_2]^{2+}$, $[Ru(H_2L')_3]^{2+}$, $[Ru(H_2L')_2(CN)_2]^0$, and $[Ru(H_2L')_2(NCS)_2]^0$. The protonation states depicted are for the dyes in powder form; the actual dye protonation states are dependent on solvent conditions. For the $Ru(bpy)_3^{2+}$-type dyes, the abbreviations used for deprotonated species in ethanol ($[Ru(L'')L_2]^+$, $[Ru(L')L_2]^0$, or $[Ru(HL')_2(H_2L')]^0$) are given in parentheses.

phosphonates[9,10] have been used in DSSCs, $[Ru(H_2L')_2(NCS)_2]^0$ and other closely related compounds have yielded the highest efficiencies reported to date in solar cell devices.[11] This enhanced efficiency is a result of the good overlap with the solar spectrum, the favorable positioning of both the ground-state and excited-state potentials of the dye relative to the redox couple in solution and to the TiO_2 conduction band edge, and the facile interfacial electron injection dynamics relative to the back-reaction rates in the cell.

One of the key features responsible for the high efficiencies of the $TiO_2/[Ru(H_2L')_2(NCS)_2]^0$ photoelectrode system is the ultrafast electron injection from the excited state of the dye into the semiconductor particles.[12,13] The chemical factors that produce such rapid electron injection have not yet been fully elucidated. Differences in the modes of binding of the dye to the semiconductor are likely to influence the electronic coupling between the dye and the semiconductor, thereby affecting the dynamics of both injection and recombination of the charge-separated state of the dye/TiO_2 moieties.[14−16] Accordingly, we have investigated the binding of dyes to nanocrystalline TiO_2 as a function of the number of anchoring groups and the type of auxiliary ligands on the metal complex. Three of the dyes investigated are ruthenium trisbipyridine derivatives, $[Ru(H_2L')_3]^{2+}$, $[Ru(H_2L')L_2]^{2+}$, and $[Ru(HL'')L_2]^{2+}$ where L is 2,2′-bipyridine, H_2L' is 4,4′-dicarboxylic acid-2,2′-bipyridine, HL″ is 4-carboxylic acid-4′-methyl-2,2′-bipyridine, and L′ and L″ are the corresponding deprotonated carboxylate bipyridine ligands (Figure 1). These dyes will be referred to collectively as $Ru(bpy)_3^{2+}$-type dyes and differ structurally only in the number of carboxy groups. The complexes $[Ru(H_2L')_2(CN)_2]^0$ and $[Ru(H_2L')_2(NCS)_2]^0$, which contain four carboxy groups, were also studied, and differ from the $Ru(bpy)_3^{2+}$-type dyes in the replacement of one bipyridine ligand with more electron rich auxiliary ligands. The protonation state of all dyes will be described throughout using the appropriate number of protons on the ligands as well as the resulting overall charge of the dye based on the solvent conditions or, in the case of sensitized TiO_2 slides, based on the solvent conditions in which binding was performed.

CHART 1: Binding Modes[a]

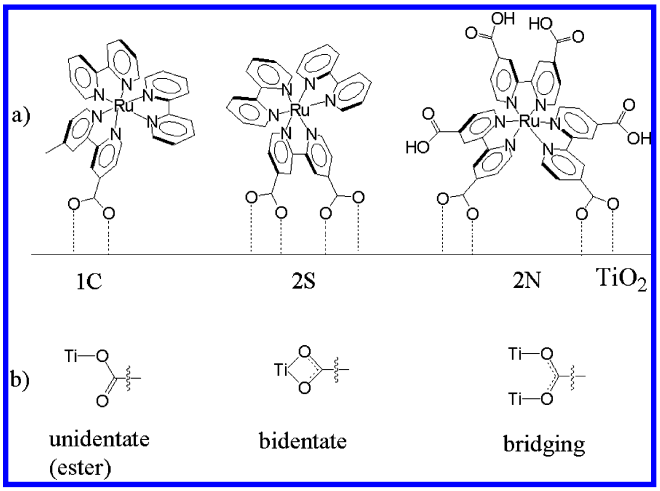

[a] 1C indicates binding through a single carboxy group; 2S indicates binding through two carboxy groups located on the same bipyridine ligand; 2N indicates binding through two carboxy groups located on neighboring bipyridine ligands. In all cases, a single carboxy group can bind in a unidentate (ester), bidentate, or bridging mode.

Several binding modes are possible for dyes that use carboxy groups to anchor to TiO_2. For example, either one (ester linkage) or both (carboxylato linkage) oxygen atoms in the carboxy group can bind to either one or two titanium atoms (Chart 1b). If only one carboxy group (1C) is attached, the binding is expected to be rather flexible. In contrast, dyes with two carboxy groups binding from the same (2S) or from neighboring (2N) bipyridine ligands are expected to produce a more robust linkage to the surface (Chart 1a). The $[Ru(H_2L')_2(CN)_2]^0$, $[Ru(H_2L')_2(NCS)_2]^0$, and $[Ru(H_2L')_3]^{2+}$ dyes can in principle access all of the suggested binding modes, whereas $[Ru(H_2L')L_2]^{2+}$ can poten-

tially bind through either the 1C or 2S modes, but $[Ru(HL'')L_2]^{2+}$ can only bind through the 1C mode (Chart 1a). The nature of the binding has been evaluated using infrared spectroscopy, and the thermodynamics and kinetics of binding have been measured on nanocrystalline TiO_2 for each member of the series. We have also investigated the influence of protonation of the carboxy moieties on the various binding properties of the metal complexes to TiO_2 and have elucidated the effect of variations in binding mode and binding constant on the performance of DSSCs.

II. Experimental Section

II.A. Materials. Acetonitrile (Merck) was freshly distilled over calcium hydride prior to use, ethanol (EtOH) (Aapor) and anhydrous pyridine (py) (Aldrich) were used as received, and 17.8 MΩ cm resistivity water was obtained from a Barnstead NANOpure filtration system. Lithium iodide (Aldrich) and anhydrous lithium perchlorate (J. T. Baker) were stored under N_2(g), iodine (Alfa-Aesar) was sublimed under vacuum and stored under N_2(g), and pyridinium triflate (pyH^+) (Aldrich) was recrystallized from diethyl ether and stored in an inert atmosphere until use.

The $[Ru(H_2L')_2(CN)_2]^0$ and $[Ru(H_2L')_2(NCS)_2]^0$ complexes were used as received from Solaronix, and $[Ru(H_2L')L_2](PF_6)_2$ and $[Ru(H_2L')_3](PF_6)_2$ were synthesized as described previously.[17] The ligand H_2L'' was prepared by oxidation of 4,4′-dimethyl-2,2′-bipyridine.[18] The $[Ru(HL'')L_2](PF_6)_2$ complex was synthesized in the same manner as $[Ru(H_2L')L_2](PF_6)_2$ except that L″ was substituted for L′ in the synthesis.[17] The counterion for all $Ru(bpy)_3^{2+}$-type dyes was PF_6^- except in the binding kinetics experiments involving $[Ru(H_2L')L_2]^{2+}$, in which case the counterion was Cl^-.

Nanocrystalline titanium dioxide films (thickness 7 ± 1 μm, crystallite size ∼15 nm) deposited by screen printing on conductive (SnO_2:F) glass were obtained from the Institut für Angewandte Photovoltaik, Germany. Before adsorption of sensitizers, the slides were cut into the desired size, typically 1−1.5 cm^2 in area. The conductive glass was then cleaned with acetone, and the TiO_2 electrodes were covered with several drops of freshly prepared acidic solution of 0.2 M Ti(IV)(aq) and left overnight in a sealed chamber to prevent evaporation of the solvent. After rinsing with water and ethanol, the slides were then annealed at 450 °C in air for 30 min and slowly cooled to 120 °C. The hot electrodes were then submerged into ethanolic solutions of the various complexes to be adsorbed onto the semiconductor. Sensitized slides were then rinsed with ethanol and dried under a stream of N_2(g) prior to use.

II.B. Spectroscopy. The steady-state electronic absorption spectra of the dyes in solution were obtained using a 1 cm optical path length quartz cuvette in an Agilent 8453 UV−vis diode array spectrometer. Solvents were either neat ethanol or ethanol containing 1 mM pyridine and 1 mM pyridinium triflate, with the latter denoted as buffered ethanol.

Corrected steady-state emission spectra were recorded on a Jobin Yvon/SPEX Fluorolog3 fluorimeter. The excitation wavelength was in the metal-to-ligand charge transfer (MLCT) band of the complexes. The quantum yields for emission of the dyes in solution were calculated by referencing each observed emission intensity to that of $Ru(bpy)_3Cl_2$ in degassed water, which has been reported to have an emission quantum yield of 0.042.[19] The emission lifetime of $[Ru(H_2L')_2(NCS)_2]^0$ was measured with single-photon-counting methods using a PicoQuant FluoTime200. All other time-resolved emission decays were measured in the microsecond range using a Nd:YAG laser and an optical parametric oscillator.[20]

The UV−vis and diffuse reflectance FTIR spectra of the dye sensitizers adsorbed onto TiO_2 were measured on dry films. Slides coated with TiO_2 that did not contain any adsorbed sensitizer were used for baseline spectra. The FTIR spectra were obtained using a BioRad SPC 32000 spectrometer and were analyzed using the Kubelka−Munk procedure for diffuse reflectance.[21,22]

II.C. Electrochemistry. The formal reduction potentials of the dyes in either ethanol or buffered ethanol containing 1.0 M $LiClO_4$ were measured by cyclic voltammetry (CV) or differential pulse voltammetry (DPV) using a BAS model 100B potentiostat equipped with a glassy carbon working electrode, a methanolic saturated calomel reference electrode, and a Pt flag counter electrode. The CV scan rate was 50 mV s^{-1}, and the pulse amplitude in the DPV measurements was 50 mV. The potential of the methanolic saturated calomel electrode was determined both by measurement against a standard saturated calomel electrode and by calibration relative to the formal potential of ferrocene in ethanol obtained from a CV scan. The formal reduction potential data obtained from the DPV measurements are reported versus a standard calomel electrode (SCE).

Photoelectrochemical cell characteristics were recorded in acetonitrile containing 0.50 M LiI, 0.040 M I_2, 0.020 M pyridine, and 0.020 M pyridinium triflate as the electrolyte using a BAS 100B potentiostat connected to a custom-designed three-electrode cell.[20] The illuminated area of the TiO_2 was 0.25 cm^2, and the measured currents are reported herein as the resultant current densities. The $J-E$ characteristics were measured either at constant photocurrent density or at 100 mW cm^{-2} of a simulated air mass (AM) 1.0 spectrum produced by an Oriel Inc. solar simulator. All samples had approximately the same coverage as determined by the absorbance (0.7 ± 0.1) at the MLCT maximum with correction for the differences in extinction coefficients. The measurements were performed versus a platinum wire in solution with a 20 mV s^{-1} scan rate. The cell resistance (65 ohms) was measured by replacing the TiO_2 electrode with a platinum foil working electrode, and the $J-E$ data were corrected for this ohmic resistance, but no corrections were made for any concentration overpotentials. The integrated quantum yields, Φ, were calculated as the ratio of the observed J_{sc} to the value expected for a unity quantum yield when the measured absorbance of the dyes on TiO_2 electrodes was convoluted with the spectral irradiance of the solar simulator between 360 and 1100 nm.

II.D. Binding Isotherms and Kinetics. Isotherms for adsorption of the various dyes were measured on 1.3−1.7 cm^2 TiO_2-coated glass slides that had been placed in 8 mL of an ethanol or buffered ethanol solution of predetermined dye concentration. The solutions were sealed and kept in the dark for 10 days. The slides were subsequently removed, rinsed with ∼0.5 mL of ethanol, and dried in air. The absorbance of the slide was then measured, and separately the washing solution was combined with the remaining dye solution. The solution was then diluted to 10 mL, after which the dissolved dye concentration was determined using optical spectroscopy. For all data reported herein, the amount of adsorbed dye (in nmol) was calculated per cm^2 of projected TiO_2 area. The extinction coefficients of the $Ru(bpy)_3^{2+}$-type dyes at the MLCT absorption maximum are 1.4×10^4 M^{-1} cm^{-1},[8] and those of the lowest energy electronic absorption in $[Ru(H_2L')_2(CN)_2]^0$ and $[Ru(H_2L')_2(NCS)_2]^0$ are 1.25×10^4 M^{-1} cm^{-1}.[17]

The kinetics of dye adsorption were determined from optical absorption measurements on dye-covered TiO_2 slides. In this

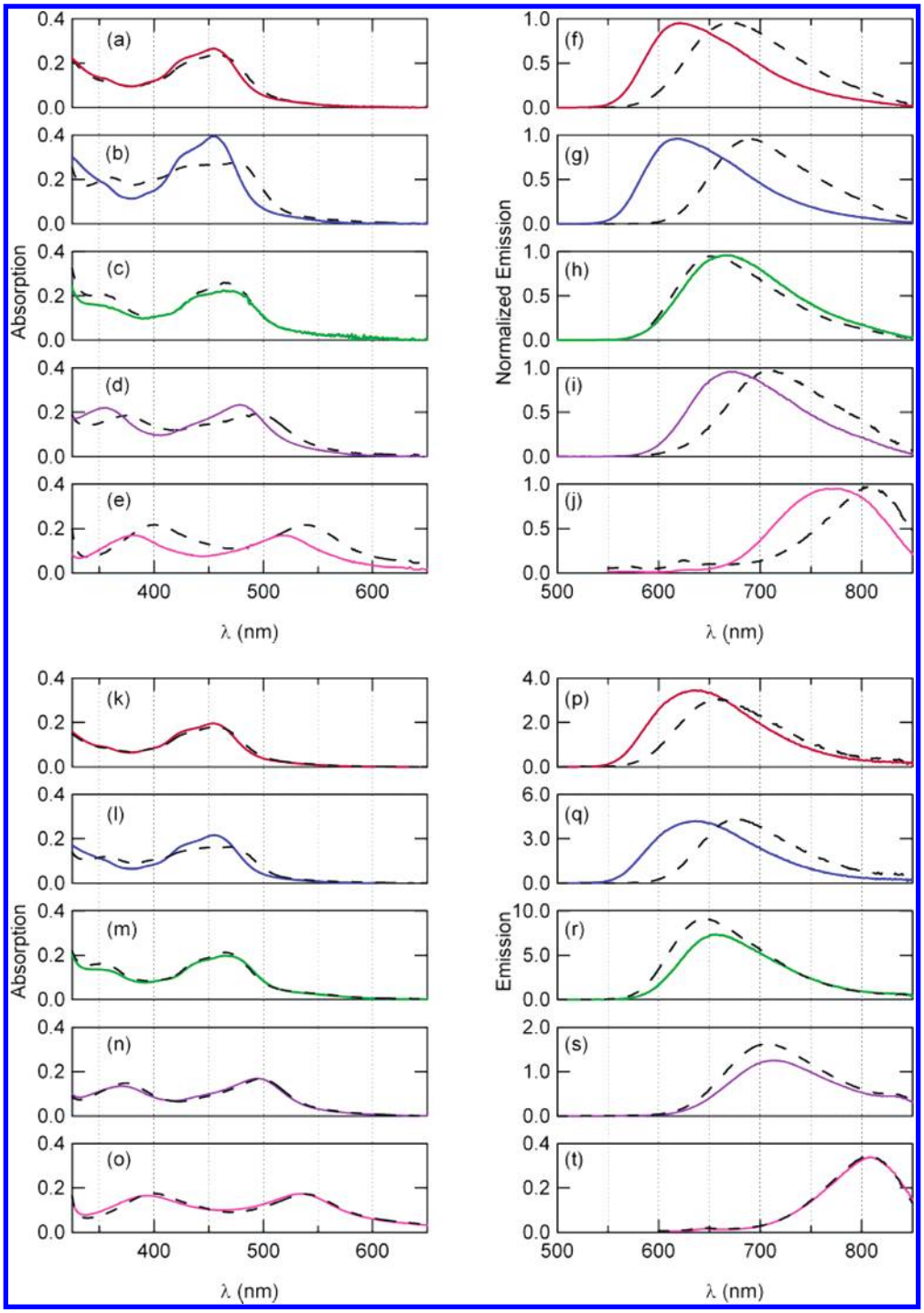

Figure 2. Spectroscopic characterization of the dyes. In each case, the initial state was the fully protonated powder: $[Ru(HL'')L_2]^{2+}$ (red; a, f, k, and p); $[Ru(H_2L')L_2]^{2+}$ (blue; b, g, l, and q); $[Ru(H_2L')_3]^{2+}$ (green; c, h, m, and r); $[Ru(H_2L')_2(CN)_2]^0$ (purple; d, i, n, and s); and $[Ru(H_2L')_2(NCS)_2]^0$ (pink; e, j, o, and t). Top panels: Absorption (a−e) and normalized corrected emission (f−j) spectra in basic (solid curve, colored) and acidic (dashed curve, black) ethanol containing a few drops of concentrated NH_3 or HCl, respectively. Lower panels: Absorption (k−o) and corrected emission (p−t) spectra in neat (solid curve, colored) and buffered (dashed curve, black) ethanol, respectively. In panels p−t, the relative emission intensities are shown.

approach, a slide was removed from the solution, rinsed and dried, taking care to minimize changes in solution volume. After each measurement, the slide was again immersed into the dye solution and the time recorded until the next measurement. The slide absorbances were converted into coverages (nmol cm^{-2} of projected area) using the relationship established in the isotherm experiments. The desorption kinetics were determined in a similar fashion but with measurement of the optical absorbance of the solution instead of the slides. In this approach, the dye-covered slides were transferred to pure ethanol, and, at desired time-points, an aliquot was transferred to a 1 cm path length cuvette. After measurement, the aliquot was reinjected into the remaining desorption solution.

III. Results

III.A. Characterization of the Dyes. Figure 2 displays the absorption (Figure 2k−o) and emission (Figure 2p−t) spectra of the dyes in neat ethanol solution. The absorption spectra of the $Ru(bpy)_3^{2+}$-type dyes exhibited a broad MLCT absorption

TABLE 1: Spectroscopic and Electrochemical Data

dye	solvent	$\lambda_{max}^{absMLCT}$ (nm)	λ_{max}^{ems} (nm)	φ_{ems} (%)	τ_{ems} (μs)	$\mathbf{E}_{00}$[a] (eV)	$E^{o\prime}$[b] (V vs SCE)	$E^{o\prime *}$[c] (V vs SCE)
$[Ru(HL'')L_2]^{2+}$	EtOH/py/pyH$^+$	455	661	4	0.8	2.11	1.03	−1.08
$[Ru(L'')L_2]^{+}$	EtOH	454	621	5	1.0	2.24		
$[Ru(H_2L')L_2]^{2+}$	EtOH/py/pyH$^+$	469	676	5	0.8	2.00	1.09	−0.99
$[Ru(L')L_2]^{0}$	EtOH	455	636	7	1.1	2.24		
$[Ru(H_2L')_3]^{2+}$	EtOH/py/pyH$^+$	465	650	11	1.6	2.11	1.30[d]	−0.81
$[Ru(HL')_2(H_2L')]^{0}$	EtOH	465	656	7	1.3	2.08		
$[Ru(H_2L')_2(CN)_2]^{0}$	EtOH/py/pyH$^+$	498	706	1.5	0.3	1.95	0.91	−1.04
$[Ru(H_2L')_2(CN)_2]^{0}$	EtOH	495	713	1	0.2	1.94		
$[Ru(H_2L')_2(NCS)_2]^{0}$	EtOH/py/pyH$^+$	538	809	0.2	0.007	1.72	0.53	−1.19
$[Ru(H_2L')_2(NCS)_2]^{0}$	EtOH	535	808	0.2	0.006	1.72		

[a] Obtained by fitting the emission spectra to the theoretical expression of Caspar et al.[26] [b] Determined from DPV measurements in buffered ethanol. [c] Calculated according to eq 1. [d] In ethanol with pyH$^+$.

band near 460 nm (Figure 2k−m, Table 1) and a $\pi-\pi^*$ ligand-based absorption band at approximately 290 nm.[23] The $[Ru(H_2L')_3]^{2+}$ complex exhibited a slightly red-shifted spectrum, with a longer tail than the other two $Ru(bpy)_3^{2+}$-type dyes. The MLCT region in the spectra of $[Ru(H_2L')_2(CN)_2]^0$ and $[Ru(H_2L')_2(NCS)_2]^0$ was split into two bands having approximately equal intensities (Figure 2n−o). Of all the dyes, $[Ru(H_2L')_2(NCS)_2]^0$ had the most red-shifted absorption spectrum.

Emission assigned to the ^{3}MLCT state of each $Ru(bpy)_3^{2+}$-type dye occurred between 600 and 700 nm (Figure 2p−r, Table 1). The emission of $[Ru(H_2L')L_2]^{2+}$ was red-shifted compared to that of $[Ru(HL'')L_2]^{2+}$, consistent with a decrease in the energy of the ligand π^* orbital due to the electron-withdrawing properties of the carboxylate.[23] The emission of $[Ru(H_2L')_2(CN)_2]^0$ and especially of $[Ru(H_2L')_2(NCS)_2]^0$ was red-shifted (Figure 2s−t), and much weaker, than that of the $Ru(bpy)_3^{2+}$-type dyes, consistent with sigma donation from CN^- and NCS^- stabilizing the "Ru(III)" center in the MLCT excited state.[24]

With the exception of $[Ru(H_2L')_3]^{2+}$, all of the dyes showed shifts in both absorption and emission when the proton activity of the solvent was changed (Figure 2a−j). Specifically, the MLCT absorption band of $[Ru(H_2L')L_2]^{2+}$ became broader and a shoulder appeared on the $\pi-\pi^*$ band when the solvent was changed from basic ethanol to acidic ethanol (Figure 2b). Only minor effects on the spectra of $[Ru(H_2L')_3]^{2+}$, $[Ru(H_2L')_2(CN)_2]^0$, and $[Ru(H_2L')_2(NCS)_2]^0$ were seen when the solvent was changed from neat to buffered ethanol (Figure 2k−t). These same spectral shifts, or lack thereof, were also seen when only pyH$^+$ was added to the solution, indicating that the buffered ethanol was acidic. The spectral data of Figure 2 indicate that all of the complexes are protonated in buffered ethanol, while $[Ru(L'')L_2]^+$ and $[Ru(L')L_2]^0$, but not $[Ru(H_2L')_2(CN)_2]^0$ or $[Ru(H_2L')_2(NCS)_2]^0$, are deprotonated in pure ethanol. $[Ru(H_2L')_3]^{2+}$ is presumably protonated in buffered ethanol and loses two protons in neat ethanol, denoted as $[Ru(HL')_2(H_2L')]^0$ (vide infra).

Both the emission quantum yield (φ) and lifetime (τ) increased in the order $[Ru(HL'')L_2]^{2+} < [Ru(H_2L')L_2]^{2+} < [Ru(H_2L')_3]^{2+}$ (Table 1). Slight changes were seen between neat and buffered ethanol, but any changes in the quantum yield were accompanied by similar changes in lifetimes. The excited-state lifetimes of the $Ru(bpy)_3^{2+}$-type dyes in neat ethanol and in buffered ethanol were ≈ 1 μs, in accord with the well-documented properties of $Ru(bpy)_3^{2+*}$.[23] The $[Ru(H_2L')_2(CN)_2]^0$ and $[Ru(H_2L')_2(NCS)_2]^0$ complexes exhibited significantly shorter excited-state lifetimes than the $Ru(bpy)_3^{2+}$-type dyes, with $\tau < 10$ ns for $[Ru(H_2L')_2(NCS)_2]^0$.[25]

Increasing the number of carboxy groups on the bipyridyl ligand shifted the M(III/II) reduction potentials ($E^{o\prime}$) of the dyes to more positive values (Table 1). In each case, the formal reduction potential for formation of M(III) from the excited state of the M(II) dye, ($E^{o\prime *}$), was calculated from eq 1:

$$E^{o\prime *} = E^{o\prime} - \mathbf{E}_{00}/q \qquad (1)$$

The energy of the 0−0 transition, $\mathbf{E}_{00}$, was determined from a fit of the emission spectrum, assuming that one bipyridyl vibrational mode of 1350 cm^{-1} was dominant (Table 1).[26] The $[Ru(H_2L')_3]^{2+*}$ species had the least negative excited-state reduction potential for formation of $[Ru(H_2L')_3]^{3+}$ ($E^{o\prime *}$, Table 1), and therefore had the lowest driving force for injection of electrons from its thermalized excited state into TiO_2.

III.B. Binding Modes. To probe for possible differences in binding modes of the various complexes, IR spectra were collected for the dyes adsorbed onto TiO_2-coated glass slides. Diffuse reflectance IR spectra could not be collected while the coated slides were in contact with solution, so all IR data were obtained on films in the dry state.

Figure 3 shows the resulting diffuse reflectance IR spectra for films prepared by adsorption of the dyes from neat ethanol. All of the dyes adsorbed under these conditions showed vibrations in the 1300−1550 cm^{-1} region from the bipyridine rings.[4] To facilitate comparison of the various spectra, the 1545 cm^{-1} ring mode was used to normalize the relative peak intensities. As expected, the $[Ru(H_2L')_2(CN)_2]^0$ and $[Ru(H_2L')_2(NCS)_2]^0$ complexes showed an absorption band near 2100 cm^{-1} that resulted from the −CN stretch of the auxiliary ligand.[27] The spectra of $[Ru(L'')L_2]^+$ and $[Ru(L')L_2]^0$ on TiO_2 contained a broad artifact between 1700 and 1900 cm^{-1} due to optical interference arising from the specific thickness of TiO_2 films used for those samples. Peaks assigned to bound carboxylato (1380 and 1610 cm^{-1}) were found for all dyes, while carbonyl stretches arising from nonbound carboxylic acids were present only for $[Ru(H_2L')_2(CN)_2]^0$, $[Ru(H_2L')_2(NCS)_2]^0$, and $[Ru(HL')_2(H_2L')]^0$ (vide infra).

III.C. Binding to TiO_2. *III.C.1. Equilibrium Binding Constants.* To elucidate how the binding properties varied with changes in the protonation state of the ligand and/or the number of ligands bound to the TiO_2 surface, the binding constants and the kinetics of binding to TiO_2 were determined for all of the dyes. Binding isotherms were measured by relating the amount of dye adsorbed on the TiO_2 to the solution equilibrium concentration (c_{eq}). Figure 4a and b display the adsorption isotherms for all the dyes bound from either neat ethanol or from buffered ethanol, respectively.

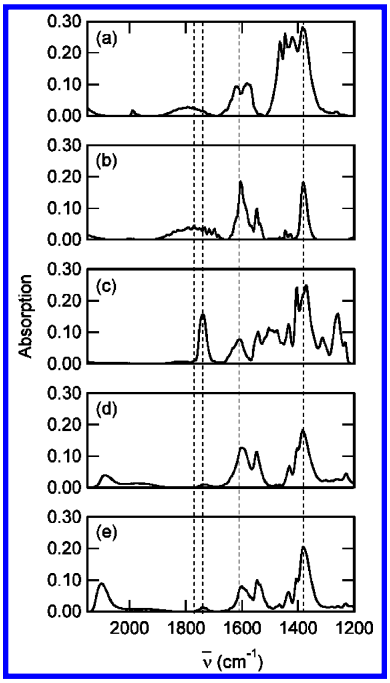

Figure 3. IR spectra on dry slides of dyes adsorbed from ethanol onto TiO_2. (a) $[Ru(L'')L_2]^+$; (b) $[Ru(L')L_2]^0$; (c) $[Ru(HL')_2(H_2L')]^0$; (d) $[Ru(H_2L')_2(CN)_2]^0$; and (e) $[Ru(H_2L')_2(NCS)_2]^0$. The dye nomenclature refers to the protonation states in ethanol, the solvent from which binding occurred. The protonation states after binding are not indicated. Dashed lines indicate the position of the key absorptions, from left to right: 1770 cm^{-1} (non-H-bonded carboxylic acid groups), 1740 cm^{-1} (H-bonded carboxylic acid groups), 1610 cm^{-1} (asymmetric bound carboxylato groups), and 1380 cm^{-1} (symmetric carboxylato groups).

Analysis of the adsorption data using a Langmuir isotherm, with the coverage (θ) given as the fraction of dye adsorbed

$$\frac{\mathrm{mol}_{\mathrm{ads}}}{\mathrm{mol}_{\mathrm{ads}}^{\mathrm{max}}} = \theta = \frac{c_{\mathrm{eq}}K_{\mathrm{ads}}}{1 + c_{\mathrm{eq}}K_{\mathrm{ads}}} \qquad (2)$$

relative to the maximum observed quantity of adsorbed dye, allowed calculation of both the maximum coverage ($\mathrm{mol}_{\mathrm{ads}}^{\mathrm{max}}$) and the adsorption constant (K_{ads}) of the various dyes onto nanocrystalline TiO_2. Table 2 and Figure 4 present the results of fitting the isotherms using eq 2 for dyes bound from ethanol or buffered ethanol. It was not possible to obtain data corresponding to $\theta \approx 1$ for $[Ru(L'')L_2]^+$ due to decreased binding of this dye, and as such, values of $\mathrm{mol}_{\mathrm{ads}}^{\mathrm{max}}$ were not reliable for this complex.

As all the dyes are of similar size, they are expected to occupy similar areas on TiO_2, in accord with the similar values of $\mathrm{mol}_{\mathrm{ads}}^{\mathrm{max}}$ obtained from analysis of the adsorption data (Table 2). The $[Ru(L'')L_2]^+$ complex exhibited a significantly lower binding constant than the other dyes, indicating that binding to TiO_2 through the monocarboxy L'' ligand is weaker than binding through the dicarboxy L' moiety. An analysis of the adsorption of $[Ru(H_2L')_2(NCS)_2]^0$ from ethanol onto TiO_2 using the Langmuir model has been reported previously,[14] and the reported K_{ads} value (0.028 μM^{-1}) is in fair agreement with our findings. In the prior work, the TiO_2 surface bonds were not activated with $TiCl_4$, which could explain the differences between the two data sets.

Langmuir analyses of the adsorption of dyes from buffered ethanol showed that $\mathrm{mol}_{\mathrm{ads}}^{\mathrm{max}}$ under such conditions was only ≈50% of the $\mathrm{mol}_{\mathrm{ads}}^{\mathrm{max}}$ values observed when the dyes were absorbed from pure ethanol. However, the adsorption constant, K_{ads}, increased significantly for all dyes when the solvent was changed from ethanol to buffered ethanol, and almost full coverage was observed at very low dye concentrations (Figure 4). Hence, the complexes were bound more strongly to the TiO_2 under more acidic conditions, but fewer sites were available on the TiO_2 surface for binding. Again the complex having the monocarboxy ligand exhibited the smallest binding constant.

The adsorption isotherms for the binding data in a specific solvent were also globally analyzed in terms of Langmuir isotherms using $\mathrm{mol}_{\mathrm{ads}}^{\mathrm{max}}$ as the global parameter (Supporting Information Table 1). Similar trends in binding constant and coverage were obtained as when the individual Langmuir analysis was used (Table 2). For very low c_{eq} values, the binding data were also analyzed according to Henry's law (Supporting Information Table 1). For low equilibrium concentrations of

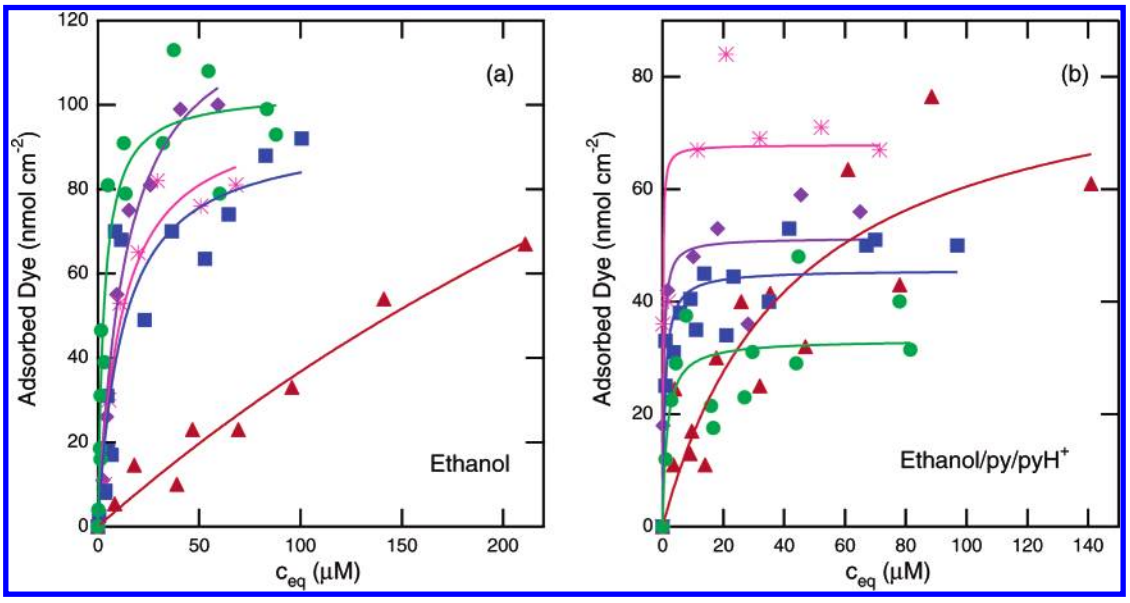

Figure 4. Binding isotherms. (a) Dye adsorption from neat ethanol of $[Ru(L'')L_2]^+$ (red, ▲); $[Ru(L')L_2]^0$ (blue, ■); $[Ru(HL')_2(H_2L')]^0$ (green, ●); $[Ru(H_2L')_2(CN)_2]^0$ (purple, ◆); and $[Ru(H_2L')_2(NCS)_2]^0$ (pink, *). (b) Dye adsorption from buffered ethanol of $[Ru(HL'')L_2]^{2+}$ (red, ▲); $[Ru(H_2L')L_2]^{2+}$ (blue, ■); $[Ru(HL')_2(H_2L')]^0$ (green, ●); $[Ru(H_2L')_2(CN)_2]^0$ (purple, ◆); and $[Ru(H_2L')_2(NCS)_2]^0$ (pink, *). Solid lines show fits to a Langmuir isotherm (eq 2).

TABLE 2: Maximum Coverages and Binding Constants for Adsorption onto Nanocrystalline TiO_2[a]

ethanol			ethanol/py/pyH$^+$		
	mol_{ads}^{max} (nmol cm^{-2})	K_{ads} (μM^{-1})		mol_{ads}^{max} (nmol cm^{-2})	K_{ads} (μM^{-1})
$[Ru(L'')L_2]^+$	270 ± 170[b]	0.002 ± 0.001	$[Ru(HL'')L_2]^{2+}$	90 ± 20	0.02 ± 0.01
$[Ru(L')L_2]^0$	90 ± 10	0.08 ± 0.03	$[Ru(H_2L')L_2]^{2+}$	50 ± 5	1 ± 0.5
$[Ru(HL')_2(H_2L')]^0$	100 ± 5	0.3 ± 0.1	$[Ru(H_2L')_3]^{2+}$	30 ± 5	0.7 ± 0.5
$[Ru(H_2L')_2(CN)_2]^0$	130 ± 10	0.09 ± 0.01	$[Ru(H_2L')_2(CN)_2]^0$	50 ± 5	3 ± 1.5
$[Ru(H_2L')_2(NCS)_2]^0$	100 ± 10	0.07 ± 0.03	$[Ru(H_2L')_2(NCS)_2]^0$	70 ± 5	8 ± 6

[a] Individual fits to one binding mode, according to a Langmuir isotherm (eq 2). [b] This value is only approximate as no data were obtainable for $\theta \approx 1$. The global Langmuir fit (Supporting Information) yielded a coverage of ≈100 nmol cm^{-2} with K_{ads} of 0.006 μM^{-1}.

TABLE 3: Nanocrystalline TiO_2 Adsorption and Desorption Kinetics

		adsorption			desorption
	solvent	dye conc (μM)	k_{ads} ($mM^{-1}\ h^{-1}$)	k_{des} (h^{-1})	$t_{1/2}$[a] (h)
$[Ru(L'')L_2]^+$	EtOH	20−125	<3[b]	≈0.3[c]	1
$[Ru(L')L_2]^0$	EtOH	10−100	7[d]	<0.04[e]	35
$[Ru(HL')_2(H_2L')]^0$	EtOH	10−100	10[d]	<0.04[e]	>100
$[Ru(H_2L')_2(CN)_2]^0$	EtOH	10−100	8[d]	<0.04[e]	>100
$[Ru(H_2L')_2(NCS)_2]^0$	EtOH	10−110	5[d]	<0.03[e]	>100
$[Ru(H_2L')_2(NCS)_2]^0$	EtOH/py/pyH$^+$	10−110	11[d]	<0.04[e]	>100

[a] Half-life for desorption; determined at the highest dye concentration. Uncertainties <10%. [b] Estimated from k_{obs} at the highest dye concentration. [c] k_{des} estimated from the average value of k_{obs}. [d] k_{ads} determined from the slope of a plot of k_{obs} vs dye concentration; uncertainties are ≈15%. [e] Estimated from k_{obs} at the lowest dye concentration.

dye in the solution, it is reasonable to assume that only the most favorable binding site will be occupied. The trends in binding constants for the different dyes were the same as those reported in Table 2 regardless of whether the Langmuir or Henry's law approach was used to analyze the data, with the L'' ligand exhibiting much weaker binding than the L' ligands and with all of the complexes exhibiting larger K_{ads} values in buffered ethanol than in pure ethanol.

III.C.2. Kinetics of Adsorption and Desorption of the Various Dyes on TiO_2. Figures 5a−c and 6a−c show data for the kinetics of binding of the various dyes to TiO_2. In each system, three different initial dye concentrations, chosen to produce a range of coverages at the end points of the adsorption process, were used for data collection.

The data for each initial dye concentration were fitted to a pair of differential equations that arise from the Langmuir isotherm model:

$$r_{ads} = \frac{d\theta}{dt} = k_{ads} c_{dye}(1 - \theta) \quad (3a)$$

$$r_{des} = \frac{d\theta}{dt} = k_{des}\theta \quad (3b)$$

$$r_{total} = r_{ads} - r_{des} \quad (3c)$$

This treatment yielded values for the sum of the rates constants, $k_{obs} = k_{ads}C_{dye} + k_{des}$, as well as K_{ads}. Plots of the sum of the rates vs C_{dye} gave straight lines (slope = k_{ads}) with near zero intercepts ($k_{des} \ll k_{ads}C_{dye}$) for all complexes except $[RuL''L_2]^+$, which showed little dependence on C_{dye} ($k_{dye} > k_{ads}C_{dye}$). For $[RuL''L_2]^+$, the value for k_{des} is the average of the k_{obs} values. For the other dyes, use of the K_{ads} values to calculate k_{des} was unreliable so limits on k_{des} were obtained from the values of k_{obs} at the lowest concentration of the dye. The results of the fitting are tabulated in Table 3 and Table SI 2.

In general, the rate constants of dye adsorption were similar for all of the dyes and additionally were similar in ethanol and buffered ethanol (Table 3). However, the adsorption kinetics of $[Ru(L'')L_2]^+$ were slightly slower than the adsorption kinetics for the other dyes binding to TiO_2 in ethanol.

Significant differences were observed in the rates of desorption of the various dyes from TiO_2. Figures 5d−f and 6d−f display the desorption kinetics of the dyes, with data collection starting from TiO_2 films having maximum dye coverage. Because the total amount of dye desorbed varied significantly, the time required for 50% of the dye to desorb, $t_{1/2}$, provided a more consistent measure of the actual desorption dynamics (Table 3) than did evaluation of trends in k_{des}. Desorption from TiO_2 of $[Ru(HL')_2(H_2L')]^0$, $[Ru(H_2L')_2(CN)_2]^0$, and $[Ru(H_2L')_2(NCS)_2]^0$ in ethanol, as well as desorption from TiO_2 of $[Ru(H_2L')_2(NCS)_2]^0$ in buffered ethanol, required $t_{1/2} > 100$ h, suggesting that binding to TiO_2 was similar for the dyes having four and six carboxy groups. In contrast, the complex with only one carboxy group, $[Ru(L'')L_2]^+$, desorbed much more rapidly and additionally produced a higher concentration of desorbed species than the other dyes. The behavior of the $[Ru(L')L_2]^0$ complex was between that of $[Ru(L'')L_2]^+$ and $[Ru(HL')_2(H_2L')]^0$ both in terms of the amount of dye desorbed and the rate of dye desorption.

III.D. Photoelectrochemical Cell Properties. Significant differences were observed in photoelectrochemical performance for the different dye-sensitized photoelectrodes in contact with 0.50 M LiI, 0.040 M I_2, 0.020 M pyridine, and 0.020 M pyridinium triflate (Figure 7a, Table 4). Spectral response measurements indicated that the steady-state short-circuit quantum yields for photocurrent flow from TiO_2 photoelectrodes coated with $[Ru(H_2L')_2(NCS)_2]^0$, $[Ru(H_2L')_2(CN)_2]^0$, or $[Ru(HL')_2(H_2L')]^0$ were all approximately 1.0 (Table 4) for excitation in the MLCT bands of the adsorbed dyes. Hence the larger short-circuit photocurrent densities, J_{sc}, produced by adsorption of $[Ru(H_2L')_2(CN)_2]^0$ or $[Ru(H_2L')_2(NCS)_2]^0$ on TiO_2 (Figure 7a) arose primarily from the enhanced spectral overlap of these dyes with the AM 1.0 solar spectrum relative to that of $[Ru(HL')_2(H_2L')]^0$ (Figure 2). For the $Ru(bpy)_3^{2+}$-type dyes, the photoelectrodes had approximately the same absorbance in the MLCT band (0.7 ± 0.1) and had similar overlap with the AM

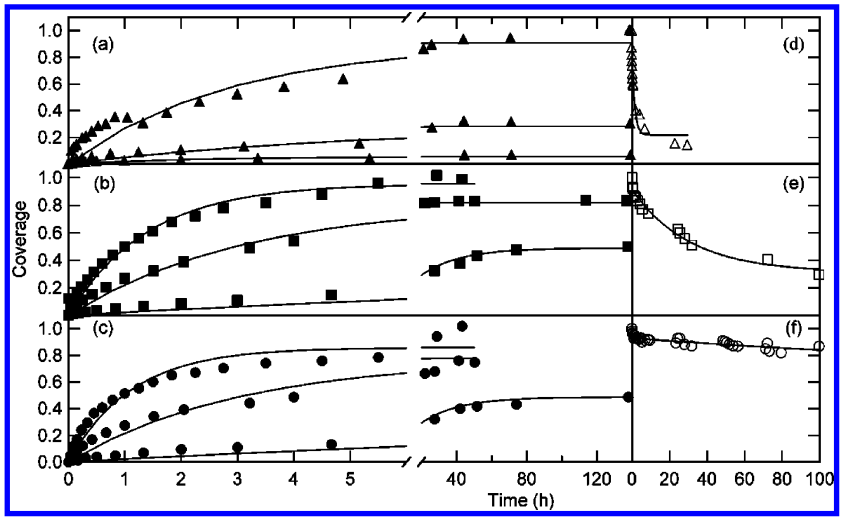

Figure 5. Kinetics of dye adsorption (a−c) and desorption (d−f) to TiO_2 from neat ethanol. Dyes and initial concentrations for adsorption are as follows: (a) $[Ru(L'')L_2]^+$ (▲) 125 μM, 55 μM, and 20 μM (top to bottom); (b) $[Ru(L')L_2]^0$ (■) 100 μM, 50 μM, and 10 μM (top to bottom); (c) $[Ru(HL')_2\ (H_2L')]^0$ (●) 100 μM, 50 μM, and 10 μM (top to bottom). The desorption kinetics (open symbols) are shown for fully covered slides: (d) $[Ru(L'')L_2]^+$; (e) $[Ru(L')L_2]^0$; (f) $[Ru(HL')_2\ (H_2L')]^0$. The lines show fits to eq 3c for the adsorption kinetics and to one or two exponential decays for the desorption kinetics.

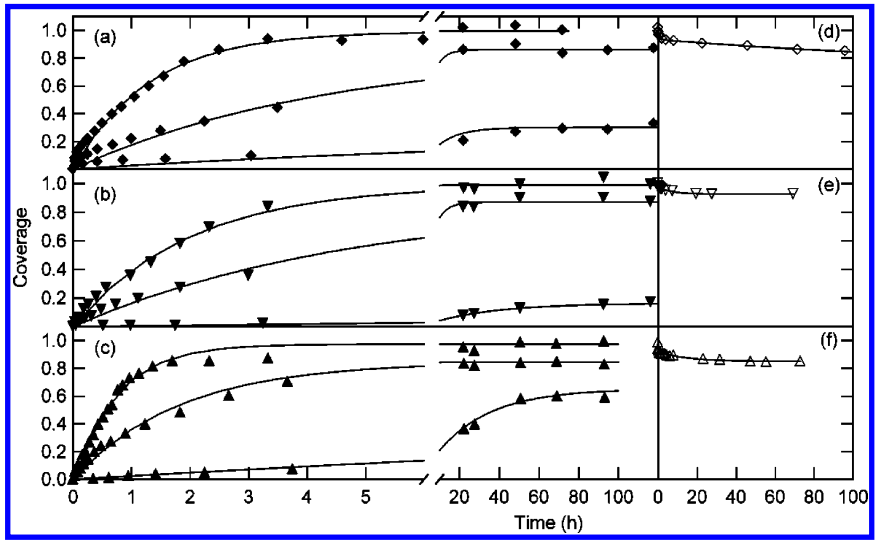

Figure 6. Kinetics of dye adsorption (a−c) and desorption (d−f) to TiO_2. Dye and initial concentrations for adsorption are as follows: (a) $[Ru(H_2L')_2(CN)_2]^0$ in neat ethanol (◆) 100 μM, 50 μM, and 10 μM (top to bottom); (b) $[Ru(H_2L')_2(NCS)_2]^0$ in neat ethanol (▼) 110 μM, 60 μM, and 10 μM (top to bottom); (c) $[Ru(H_2L')_2(NCS)_2]^0$ in buffered ethanol (▲) 110 μM, 60 μM, and 10 μM (top to bottom). The desorption kinetics (open symbols) are shown for fully covered slides: (d) $[Ru(H_2L')_2(CN)_2]^0$; (e) $[Ru(H_2L')_2(NCS)_2]^0$ (bound from neat ethanol); (f) $[Ru(H_2L')_2(NCS)_2]^0$ (bound from buffered ethanol). The lines show fits to eq 3c for the adsorption kinetics and to two exponential decays for the desorption kinetics.

1.0 spectrum, so any significant differences in J_{sc} or photoelectrode energy conversion efficiency between dyes in this series were not due to differences in light absorption. For the $Ru(bpy)_3^{2+}$-type dyes, the J_{sc} values and integrated quantum yields decreased in the order $[Ru(HL')_2(H_2L')]^0 > [Ru(L')L_2]^0 > [Ru(L'')L_2]^+$. The $[Ru(L'')L_2]^+$ system additionally exhibited significant variability in photoelectrode performance.

Electrochemical measurements of the dye-coated photoelectrodes in the absence of illumination were performed to investigate the rate of reaction of electrons in TiO_2 with the redox couple in solution (Figure 7b). The relative rates of this reaction for different dyes can be inferred from the dark current density as a function of electrode potential. Less negative potentials required to drive the same current density in the dark indicate more facile electron transfer processes between TiO_2 and oxidized species in the electrolyte. Because the dyes produced similar surface coverages, similar rates of back electron transfer from reduced TiO_2 to the redox couple in solution would be expected for all the systems. However, all of the $Ru(bpy)_3^{2+}$-type dyes showed an enhanced dark current density compared to $[Ru(H_2L')_2(CN)_2]^0$ and $[Ru(H_2L')_2(NCS)_2]^0$. A TiO_2 slide without dye showed the largest dark current density under these conditions. Furthermore, in the case of $[Ru(L'')L_2]^+$, the average dark current density was significantly greater than that observed for the other two $Ru(bpy)_3^{2+}$-type dyes. Consistently, the open-circuit voltages, V_{oc}, were quite similar for $[Ru(HL')_2(H_2L')]^0$ and $[Ru(L')L_2]^0$ and were lower (less negative) for $[Ru(L'')L_2]^+$ (Table 4). No significant difference was observed in the photoelectrochemical response between dyes adsorbed onto the TiO_2 from buffered ethanol relative to dyes adsorbed from pure ethanol.

IV. Discussion

IV.A. Characterization of the Dyes. A comparison between the spectra in neat and buffered ethanol (Figure 2k−t) with the

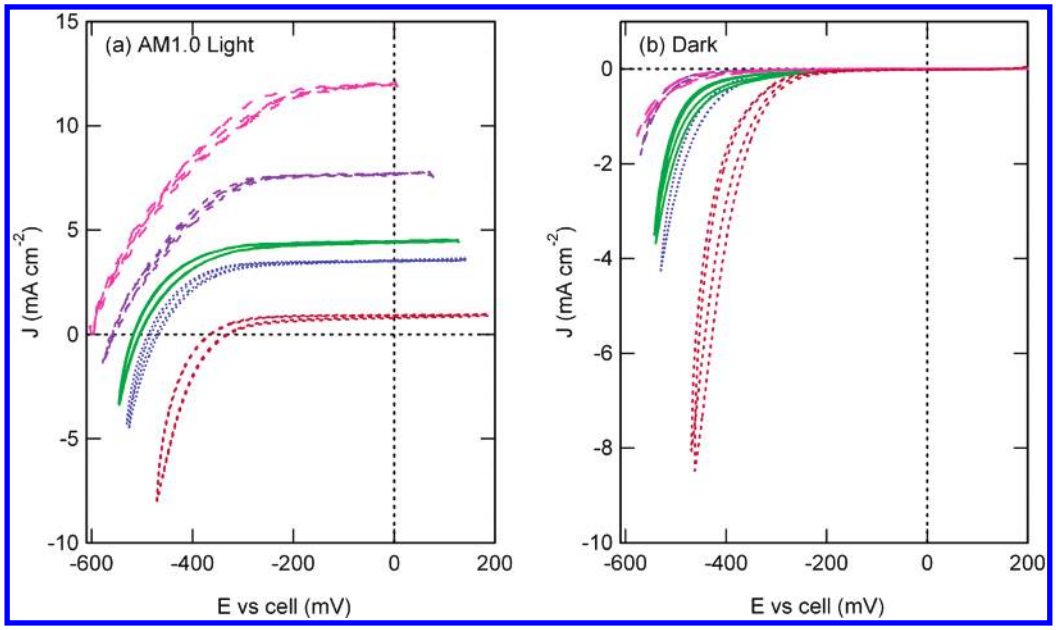

Figure 7. Current density vs potential behavior for nanocrystalline TiO_2 photoelectrodes sensitized with adsorbed dyes in contact with 0.50 M LiI, 0.040 M I_2, 0.020 M py, and 0.020 M pyH^+ in acetonitrile. Sensitizers adsorbed from ethanol are as follows: $[Ru(L'')L_2]^+$ (red, dashed curve); $[Ru(L')L_2]^0$ (blue, dotted curve); $[Ru(HL')_2\ (H_2L')]^0$ (green, solid curve); $[Ru(H_2L')_2(CN)_2]^0$ (purple, large dashed curve); and $[Ru(H_2L')_2(NCS)_2]^0$ (pink, dash-dot-dash curve). Dye nomenclature refers to the protonation states in neat ethanol, the solvent from which binding occurred. (a) $J-E$ behavior under simulated air mass 1.0 (100 mW cm^{-2}) conditions. (b) $J-E$ behavior in the dark.

TABLE 4: Photoelectrochemical Cell Characteristics under Simulated Solar Illumination

	J_{sc}[a] (mA cm^{-2})	V_{oc}[a] (V)	ff[b]	efficiency[c] (%)	Φ[d]	dark voltage[e] (V)
$[Ru(L'')L_2]^+$	1.5 ± 1	-0.38 ± 0.1	0.7	0.2	0.37	-0.33 ± 0.1
$[Ru(L')L_2]^0$	3 ± 0.5	-0.48 ± 0.05	0.5	0.7	0.66	-0.42 ± 0.05
$[Ru(HL')_2(H_2L')]^0$	4 ± 0.5	-0.49 ± 0.05	0.6	1.1	0.95	-0.44 ± 0.05
$[Ru(H_2L')_2(CN)_2]^0$	6 ± 2	-0.52 ± 0.05	0.6	1.4	0.85	-0.51 ± 0.05
$[Ru(H_2L')_2(NCS)_2]^0$	10 ± 2	-0.56 ± 0.05	0.5	2.1	1.08	-0.51 ± 0.05

[a] Acetonitrile with 0.50 M LiI, 0.040 M I_2, 20 mM py, 20 mM pyH^+ under AM 1.0 conditions. Values are averages of measurements using five different TiO_2 electrodes. [b] The fill factor (ff) is calculated as $P_{max}/((J_{sc})(V_{oc}))$, where P_{max} is the most negative value of JV. [c] Calculated as $((-J_{sc})(V_{oc})(ff) \times 100\%)/I_{light}$, where $I_{light} = 100$ mW cm^{-2}. [d] The integrated quantum yield (Φ) was determined by comparing the experimentally measured value of J_{sc} with the maximum calculated J_{sc} assuming a unity quantum yield when the measured absorbance of the dyes on the TiO_2 electrodes are convoluted with the spectral irradiance of the solar simulator between 1100 and 360 nm. [e] Potential required to drive a cathodic current density of 0.1 mA cm^{-2} in the dark.

spectra in acidic and basic ethanol (Figure 2a−j) shows that the $[Ru(HL'')L_2]^{2+}$ and $[Ru(H_2L')L_2]^{2+}$ dyes were predominantly (>90%) protonated in buffered ethanol, whereas in neat ethanol the pendant carboxy groups of these dyes were fully deprotonated, yielding $[Ru(L'')L_2]^+$ and $[Ru(L')L_2]^0$, respectively. These protonation state assignments are consistent with the observation that the spectra of the complexes in ethanol with pyH^+ added were the same as those recorded in acidic or buffered ethanol, while the spectra in ethanol with py added were similar to those observed in neat ethanol. The red-shift upon protonation of $[Ru(H_2L')L_2]^{2+}$ is consistent with that reported for protonation of this dye in water.[28] For both $[Ru(H_2L')_2(CN)_2]^0$ and $[Ru(H_2L')_2(NCS)_2]^0$, the spectral shift upon addition of buffer (≈3 nm) was significantly smaller than the shift between fully protonated and fully deprotonated dyes (≈20 nm). For these two dyes, the spectra in both neat and buffered ethanol are consistent with complete (>90%) protonation of the pendant carboxy groups.

The spectrum of the $[Ru(H_2L')_3]^{2+}$ dye did not exhibit a significant shift between acidic and basic ethanol solutions, and the spectral features observed were located between those of the fully protonated and fully deprotonated species of the two other $Ru(bpy)_3^{2+}$-type dyes. The absorption and emission spectra of $[Ru(H_2L')_3]^{2+}$ also did not shift significantly between neat and buffered ethanol. This is consistent with the π^* orbital on the protonated ligand, H_2L', being lower in energy than that of the deprotonated ligand. Thus, for either the protonated or partially deprotonated complex, the absorption and emission involve the π^* orbital on a protonated ligand. Despite the absence of a spectral shift for this dye, $[Ru(H_2L')L_2]^{2+}$ and $[Ru(H_2L')_3]^{2+}$ exhibit similar pK_a's, and thus their protonation states in neat and buffered ethanol are expected to be similar.[28,29] This suggests that $[Ru(H_2L')_3]^{2+}$ is fully protonated in buffered ethanol and loses two protons to form $[Ru(HL')_2(H_2L')]^0$ in neat ethanol.

The small emission blue-shift in acidic media observed for $[Ru(H_2L')_3]^{2+}$ was similar to the blue-shift observed for $[Ru(H_2L')_2(CN)_2]^0$ when the solvent was changed from neat to buffered ethanol. Because this small shift for $[Ru(H_2L')_2(CN)_2]^0$ is not due to a change in protonation,[30,31] but rather to changes in media, the shift observed for $[Ru(H_2L')_3]^{2+}$ can likely be explained similarly. For the $Ru(bpy)_3^{2+}$-type dyes, the absorption and emission spectra were the same in water and ethanol. For $[Ru(H_2L')_2(CN)_2]^0$ and $[Ru(H_2L')_2(NCS)_2]^0$, both absorption and emission spectra were significantly blue-shifted (≈20 nm) in water relative to ethanol, possibly as a result of specific solvation of the CN^- and SCN^- ligands.[31−35]

IV.B. Binding Modes. Unprotonated carboxylate or bound carboxylato groups exhibit symmetric and asymmetric stretches at ≈1380 and ≈1610 cm^{-1}, respectively, whereas the carbonyl stretches associated with free carboxylic acids appear at ≈1740 cm^{-1} for H-bonded acid groups and at ≈1770 cm^{-1} for non-H-bonded acid groups.[4,36] The IR bands associated with bound carboxylato and nonbound carboxylate groups are expected to be very close to 1600 cm^{-1}, so the IR spectra do not allow facile differentiation between these two groups. All of the complexes bound to TiO_2 exhibited IR stretches at ≈1380 and ≈1610 cm^{-1} (Figure 3).

The splitting observed between the symmetric and asymmetric carboxylato stretches (≈230 cm^{-1}) of all of the complexes bound to TiO_2 is close to the splitting reported for the ionic species $[Ru(L')_2(NCS)_2]^{4-}$ (≈250 cm^{-1}).[4] A much larger separation between the symmetric and asymmetric carboxylato stretching frequencies is expected in unidentate ester linkages, due to the different environments of the two oxygens in the ester group.[4,37] Such a large separation was not observed in any of the IR spectra recorded in this work. Thus the observed splitting indicates that in the dry state, the carboxylato groups used both oxygen atoms to attach to either one (i.e., the bidentate binding mode) or two (i.e., the bridging binding mode) titanium atoms. Furthermore, the lack of a significant shift between the stretching frequency observed for the bound carboxylato groups and that observed for ionic carboxylates in solution (1588 and 1387 cm^{-1}) suggests that the complexes predominantly used the bridging mode of binding.[36,38]

The bound $[Ru(H_2L')_2(CN)_2]^0$, $[Ru(H_2L')_2(NCS)_2]^0$, and $[Ru(HL')_2(H_2L')]^0$ complexes additionally exhibited a spectral feature at 1740 cm^{-1} attributable to carbonyl stretches arising from protonated carboxylic acids. The ratio of bound carboxylato to protonated (nonbound) carboxylic acid groups can be estimated from the ratio of the intensities of the bands corresponding to carboxylato stretches (1610 cm^{-1}) relative to those corresponding to nonbound acids (1740 cm^{-1}).[4] For binding of either $[Ru(H_2L')_2(CN)_2]^0$ or $[Ru(H_2L')_2(NCS)_2]^0$ to TiO_2, a series of trials resulted in a mean ratio of the intensity at 1740 cm^{-1} to that at 1610 cm^{-1} of 1.0 ± 0.5. Assuming that all the carboxylato and carboxylic acid groups are bound and unbound, respectively, either a 2:2 or 3:1 ratio of bound to unbound carboxy groups is compatible with the IR intensity data. Individual molecules may bind through a mixture of binding modes with, for example, one molecule attached to the surface with three carboxylato groups.

For binding of $[Ru(HL')_2(H_2L')]^0$ to TiO_2, the ratio of the absorption intensities at 1740 and 1610 cm^{-1} was ≈2, consistent with this species having twice as many protonated as unprotonated groups (4 carboxylic acids:2 carboxylato groups). This intensity ratio therefore suggests that on average only two of the six carboxy groups are used in binding this dye to TiO_2. For the two remaining dyes, $[Ru(HL'')L_2]^{2+}$ and $[Ru(H_2L')L_2]^{2+}$, the 1740 cm^{-1} band assigned to free, nonbound acid groups was less than 10% of the intensity of the 1610 cm^{-1} carboxylato stretch regardless of the initial protonation state of the dye in the binding solution, that is, binding from buffered (protonated) or neat (deprotonated) ethanol. This suggests that all of the available carboxy groups (one or two, respectively) in these two dyes are used in binding to TiO_2.

Previous work has shown that even when a fully deprotonated dye in solution binds to TiO_2, the nonbound acid groups are protonated due to deprotonation of the TiO_2 surface.[4] Consistently, the IR spectra were observed to be essentially identical for dyes bound from either buffered or nonbuffered ethanolic solution, with both being indicative of protonated, nonbound carboxylic acids for bound $[Ru(H_2L')_2(CN)_2]^0$, $[Ru(H_2L')_2(NCS)_2]^0$, and $[Ru(HL')_2(H_2L')]^0$ regardless of the initial protonation state of these dyes in solution.

IV.C. Binding to TiO_2. *IV.C.1. Equilibrium Binding Constants.* The adsorption constants exhibited similar trends between the various dyes regardless of the method used to analyze the isotherm data. In the Langmuir approach, the inherent assumption based on noncooperative monolayer adsorption to chemically equivalent binding sites is likely not rigorously applicable to a heterogeneous, nanocrystalline TiO_2 system. However, fitting of the binding data to other models, such as the Freundlich isotherm or to a sum of two Langmuir isotherms, did not improve the quality of the fit, and therefore the Langmuir approach was adopted for data analysis.

On the basis of the charge of the various complexes, it is expected that the proton affinities of the carboxy groups on the $[Ru(HL')_2(CN)_2]^{2-}$ and $[Ru(HL')_2(NCS)_2]^{2-}$ dyes would be greater than those on the $Ru(bpy)_3^{2+}$-type dyes. This expectation is consistent with the absorption spectra that indicate that the $[Ru(H_2L')_2(CN)_2]^0$ and $[Ru(H_2L')_2(NCS)_2]^0$ complexes are protonated in neat ethanol, whereas the other complexes are deprotonated under these conditions and require acidic or buffered ethanol to be fully protonated. The trend in binding the various carboxy ligands to the "hard" Ti(IV) center is expected to parallel their proton affinities. This expectation is consistent with the observation that in buffered ethanol the $[Ru(H_2L')_2(CN)_2]^0$ and $[Ru(H_2L')_2(NCS)_2]^0$ complexes exhibited the largest binding constants (Table 2).

Both $[Ru(H_2L')L_2]^{2+}$ and $[Ru(HL')_3]^{2+}$ showed a significantly larger binding constant in buffered ethanol than $[Ru(HL'')L_2]^{2+}$, consistent with a chelate effect, as supported by the IR spectroscopic data for dry films of these various complexes on TiO_2. Furthermore, in neat ethanol, the three $Ru(bpy)_3^{2+}$-type dyes are deprotonated and, as expected, K_{ads} increases in the order of increasing chelate effect. Therefore, differences in their binding constants between neat and buffered ethanol could be related to charge effects. In contrast, the carboxy groups in $[Ru(H_2L')_2(NCS)_2]^0$ and $[Ru(H_2L')_2(CN)_2]^0$ are protonated in both neat and buffered ethanol, and hence the differences in binding constants are not a function of changes in the state of the dyes but must be ascribed to changes in the surface of the TiO_2.

The most dramatic changes in K_{ads} between neat and buffered ethanol were observed for $[Ru(H_2L')_2(CN)_2]^0$ and $[Ru(H_2L')_2(NCS)_2]^0$. These two dyes did not change their protonation states upon addition of py/pyH^+ to ethanol (Figure 2), indicating that the increase in K_{ads} for all of the dyes likely arose from a difference in the chemical state of the TiO_2 surface between pure and buffered ethanol. The observed behavior is consistent with the hypothesis that protons or amines interact with the TiO_2 surface, resulting in competition for dye binding that reduces mol_{ads}^{max} under more acidic conditions.

Water is released upon binding the dyes to protonated TiO_2 surfaces. For a 1.5 cm^2 area dye-covered slide, the amount of water released will be less than 400 nmol, assuming two carboxylato linkages are formed. This corresponds to ≈7 μL (50 μM) of water, which is far less than the water already present in the ethanol. Furthermore, prior work has shown that water concentrations up to 50 mM in acetonitrile do not affect the performance of TiO_2 photoelectrodes sensitized with $[Ru(H_2L')_2(NCS)_2]^0$.[39] Water release is even less significant during the binding of dyes from buffered ethanol. Hence, because the bound dye is not hydrolyzed under either of these conditions,

the binding properties reported herein should be independent of the presence of small amounts of water.

IV.C.2. Kinetics of Adsorption and Desorption of the Various Dyes on TiO_2. A striking feature of the kinetics data of Table 3 is the similarity between all of the adsorption rate constants regardless of the binding constants, desorption rates, degree of protonation, number of carboxy groups available for binding, or solvent conditions. For example, only a 2-fold increase in the adsorption rate constant was found for $[Ru(H_2L')_2(NCS)_2]^0$ when the solvent was changed from ethanol to buffered ethanol, even though the binding constant increased by a factor of $\approx 10^2$ (Table 2). Hence the variation in binding constants reported in Table 2 cannot be ascribed primarily to differences in the rate of adsorption of the various dyes. Only slightly lower rates were observed for adsorption of $[Ru(L'')L_2]^+$, suggesting that the formation of the first bond to TiO_2 is rate limiting.

The largest differences in the kinetics data for interaction of the various dyes with TiO_2 were observed in the dye desorption process (Figure 5d−f, Figure 6d−f, Table 3). The $[Ru(L'')L_2]^+$ dye, which can bind only in the 1C mode, exhibited the most rapid desorption kinetics. Furthermore, the amount of dye desorbed in ethanol was larger for $[Ru(L'')L_2]^+$ than for any of the other dyes. The $[Ru(HL')_2(H_2L')]^0$, $[Ru(H_2L')_2(NCS)_2]^0$, and $[Ru(H_2L')_2(CN)_2]^0$ complexes have two carboxy groups on each bipyridine and thus can in principle access all three binding modes. Only small amounts of these dyes were desorbed, and they showed similar desorption kinetics, indicating that dyes with four or more anchoring groups were bound similarly to TiO_2. The initial desorption rate for these complexes was almost as rapid as for $[Ru(L'')L_2]^+$, suggesting that either small amounts of these dyes bind in the 1C motif, or more likely, some bind noncovalently. Because no significant difference was observed in the binding properties of $[Ru(HL')_2(H_2L')]^0$ (six carboxy groups) from that of $[Ru(H_2L')_2(NCS)_2]^0$ or $[Ru(H_2L')_2(CN)_2]^0$ (four carboxy groups), it is likely that not all of the six $[Ru(HL')_2(H_2L')]^0$ carboxy groups bind to TiO_2, in accord with the IR spectroscopic analysis (vide supra).

Both the desorption rate and the amount of dye desorbed in ethanol for $[Ru(L')L_2]^0$ were found to be between the values for the two other $Ru(bpy)_3^{2+}$-type dyes. Because both $[Ru(HL')_2(H_2L')]^0$ and $[Ru(L')L_2]^0$ are bound through two carboxy groups according to the IR spectroscopic analysis, the differences in desorption kinetics indicate that binding through carboxy groups on neighboring bipyridines (2N) in $[Ru(HL')_2(H_2L')]^0$ is stronger and less labile than through carboxy groups on the same bipyridine (2S), the latter being the only possibility other than 1C for $[Ru(L')L_2]^0$. Molecular modeling also suggests that the 2N binding motif is sterically more favorable than that of 2S.[40] A study of a similar series of carboxylated ruthenium phenanthroline complexes also showed that one anchoring group is not sufficient to achieve good photoelectrochemical performance.[16]

IV.D. Photoelectrochemical Cell Properties. Photoelectrodes sensitized with the $[Ru(H_2L')_2(CN)_2]^0$ and $[Ru(H_2L')_2(NCS)_2]^0$ complexes exhibited the highest energy conversion efficiencies under simulated solar illumination, primarily because their absorption spectra most closely matched the spectral irradiance profile of the excitation source. The integrated quantum yield, Φ, which is independent of differences in spectral overlap, allows for a more direct comparison between the photoelectrochemical properties of these five dyes. The $[Ru(H_2L')_2(NCS)_2]^0$, $[Ru(H_2L')_2(CN)_2]^0$, and $[Ru(HL')_2(H_2L')]^0$ complexes, which can access the 2N mode with better overall binding properties than binding through the 2S or 1C mode, exhibited the highest quantum yields on TiO_2, whereas $[Ru(L')L_2]^0$, which can bind in the 2S but not the 2N mode, showed a lower quantum yield, and $[Ru(L'')L_2]^+$, which can only bind through 1C, exhibited the lowest quantum yield (Table 4). Thus, the short-circuit quantum yields for sensitizers in the $Ru(bpy)_3^{2+}$-type series declined in the order 2N > 2S > 1C, correlating with the trends in the desorption kinetics of this system.

The quantum yield is a function of the competition between a number of processes, implying that at least one of the processes correlates with the variation in binding strength and desorption dynamics in this series of adsorbed complexes. The decrease in quantum yield for adsorbed $[Ru(L'')L_2]^+$ relative to the other sensitizers is not ascribable to less favorable energetics for this complex, because this sensitizer had the most negative excited-state potential and therefore had the largest driving force of all the complexes studied in this work for injection of charge carriers into TiO_2 (Table 1). Additionally, all of the complexes have ground-state Ru(III/II) formal potentials that are sufficiently positive to oxidize the I_3^-/I^- redox system and therefore readily regenerate the reduced form of the dye (Table 1). Time-resolved spectroscopic experiments are in progress to elucidate more fully which of the fundamental rate processes, such as the electronic coupling to the semiconductor or the quenching by solution-based redox species, is most directly affected by the variation in the binding of the different dyes to the TiO_2 surface.

The photoelectrochemical behavior of the various dyes adsorbed onto TiO_2 exhibited trends in two different quantities, J_{sc} and V_{oc}, both of which contributed to changes in photoelectrode energy conversion efficiency as the adsorbed dye was varied. The open-circuit voltage also exhibited a correlation with the binding modes of the sensitizer to the TiO_2 surface. The open-circuit voltage is a photostationary state property that is primarily a function of the short-circuit current density and secondarily a function of the rate of the direct reduction of redox species in the electrolyte by electrons in the TiO_2. The effect of changes in the short-circuit current density can be removed either by comparing photovoltages at illumination intensities that produce comparable short-circuit photocurrent densities or by comparing the potentials needed to produce a constant cathodic current density in the dark. In either comparison, TiO_2 electrodes sensitized with $[Ru(H_2L')_2(NCS)_2]^0$, $[Ru(H_2L')_2(CN)_2]^0$, or $[Ru(HL')_2(H_2L')]^0$ exhibited significantly smaller direct reduction rates than did electrodes sensitized with $[Ru(L')L_2]^0$, which in turn had smaller direct reduction losses than those sensitized with $[Ru(L'')L_2]^+$. This indicates that adsorption of $[Ru(H_2L')_2(NCS)_2]^0$, $[Ru(H_2L')_2(CN)_2]^0$, or $[Ru(HL')_2(H_2L')]^0$ inhibited direct reduction of the electrolyte by the TiO_2 surface. Reducing the binding strength, and therefore producing a more labile complex, produced a higher direct reduction rate and a lower open-circuit voltage for such systems.

The temporal stability of the photoelectrodes of course should correlate to the binding strength and desorption kinetics of the various dyes. The large variance in photoelectrochemical performance that was observed when $[Ru(L'')L_2]^+$ was used to sensitize TiO_2 indicates that two or more carboxylic acids produce superior photoelectrochemical cell stabilities in this series of complexes under operating cell conditions. Hence, the linkage to the TiO_2 surface can play an important role in achieving temporal stability as well as in tuning both the steady-state quantum yield and the magnitude of the predominant back-reaction rate in dye-sensitized TiO_2-based photoelectrochemical solar cells. For the carboxylated ruthenium dyes investigated herein, both the temporal stability and photoelectrochemical

performance were correlated since binding modes that improved the temporal stability (reduced desorption rates and improved binding constant) also produced improved energy conversion performance.

V. Conclusions

For the series of carboxylated ruthenium dyes, a correlation was observed between the chemical nature of dye binding and the photoelectrochemical behavior of the resulting dye-sensitized TiO_2 electrodes. The IR spectra indicated that the dyes bound in a bridging fashion, that is, with both oxygen atoms from an anchoring carboxy group interacting with adjacent titanium atoms on the TiO_2 surface, but not all carboxy groups participated in binding to the TiO_2. Complexes having either a single monocarboxy ligand or a single dicarboxy ligand used essentially all of their carboxy groups to bind to the surface, whereas complexes having four or six carboxy groups used on average two carboxy groups in binding to TiO_2. The binding constant of $[Ru(HL'')L_2]^{2+}$ was smaller than those of all the other dyes to TiO_2, indicating that two carboxyl groups bound significantly tighter than one. The adsorption rate constants did not vary significantly among the dyes, suggesting that formation of the first bond to TiO_2 was rate limiting. The $[Ru(HL'')L_2]^{2+}$ desorbed much more rapidly and more completely than either $[Ru(H_2L')_3]^{2+}$, $[Ru(H_2L')_2(CN)_2]^0$, or $[Ru(H_2L')_2(NCS)_2]^0$, indicating that in this series of dyes, the binding constants were determined primarily by differences in the desorption process. The desorption kinetics indicated that binding to TiO_2 using two carboxyl groups on neighboring bipyridine rings (2N) was less labile than binding using groups on the same bipyridine ring (2S). Furthermore, dyes that used either the 2N or 2S binding mode desorbed significantly less rapidly than dyes that were bound through the 1C mode. TiO_2 photoelectrodes sensitized with $[Ru(H_2L')_2(CN)_2]^0$, $[Ru(H_2L')_2(NCS)_2]^0$, and $[Ru(H_2L')_3]^{2+}$ displayed integrated quantum yields that approached unity, indicating that differences in the short-circuit current density under solar illumination can be ascribed primarily to differences in overlap of these various dyes with the solar spectrum. However, the integrated quantum yields within the series of $Ru(bpy)_3^{2+}$-type complexes decreased in the order $[Ru(H_2L')_3]^{2+} > [Ru(H_2L')L_2]^{2+} \gg [Ru(HL'')L_2]^{2+}$, indicating that the short-circuit current density and steady-state quantum yield correlated with the available binding type (2N > 2S $\gg$ 1C). In addition, the dark current was largest for the monocarboxy dye that used the weakest, most labile 1C mode of binding. The $[Ru(HL'')L_2]^{2+}$ complex was significantly less stably bound to TiO_2 over time than the other dyes and consequently produced a wide range of photoelectrochemical responses. Hence, the linkage to the TiO_2 surface plays an important role in achieving temporal stability of the photoelectrochemical properties as well as in tuning both the steady-state quantum yield and the magnitude of the predominant back-reaction rate in dye-sensitized TiO_2-based photoelectrochemical solar cells.

Acknowledgment. This work was supported by BP (H.B.G; J.R.W.) and DOE/NREL (N.S.L.). K.K. thanks the Carlsberg Foundation (Denmark) for a postdoctoral fellowship.

Supporting Information Available: Analyses of equilibrium binding (global Langmuir isotherm and Henry's law) and adsorption kinetics in both neat and buffered ethanol are available. This material is available free of charge via the Internet at http://pubs.acs.org.

References and Notes

(1) O'Regan, B.; Grätzel, M. *Nature* **1991**, *353*, 737−740.
(2) Hagfeldt, A.; Grätzel, M. *Acc. Chem. Res.* **2000**, *33*, 269−277.
(3) Cahen, D.; Hodes, G.; Grätzel, M.; Guillemoles, J. F.; Riess, I. *J. Phys. Chem. B* **2000**, *104*, 2053−2059.
(4) Finnie, K. S.; Bartlett, J. R.; Woolfrey, J. L. *Langmuir* **1998**, *14*, 2744−2749.
(5) Cherepy, N. J.; Smestad, G. P.; Grätzel, M.; Zhang, J. Z. *J. Phys. Chem. B* **1997**, *101*, 9342−9351.
(6) Koehorst, R. B. M.; Boschloo, G. K.; Savenije, T. J.; Goossens, A.; Schaafsma, T. J. *J. Phys. Chem. B* **2000**, *104*, 2371−2377.
(7) Ferrere, S. *Chem. Mater.* **2000**, *12*, 1083−1089.
(8) Sauvé, G.; Cass, M. E.; Coia, G.; Doig, S. J.; Lauermann, I.; Pomykal, K. E.; Lewis, N. S. *J. Phys. Chem. B* **2000**, *104*, 6821−6836.
(9) Pechy, P.; Rotzinger, F. P.; Nazeeruddin, M. K.; Kohle, O.; Zakeeruddin, S. M.; Humphy-Baker, R.; Grätzel, M. *J. Chem. Soc., Chem. Commun.* **1995**, 65−66.
(10) Yan, S. G.; Hupp, J. T. *J. Phys. Chem.* **1996**, *100*, 6867−6870.
(11) Nazeeruddin, M. K.; Pechy, P.; Renouard, T.; Zakeeruddin, S. M.; Humphry-Baker, R.; Comte, P.; Liska, P.; Cevey, L.; Costa, E.; Shklover, V.; Spiccia, L.; Deacon, G. B.; Bignozzi, C. A.; Grätzel, M. *J. Am. Chem. Soc.* **2001**, *123*, 1613−1624.
(12) Benkö, G.; Myllyperkiö, P.; Pan, J.; Yartsev, A. P.; Sundström, V. *J. Am. Chem. Soc.* **2003**, *125*.
(13) Kuciauskas, D.; Monat, J. E.; Villahermosa, R.; Gray, H. B.; Lewis, N. S.; McCusker, J. K. *J. Phys. Chem. B* **2002**, *106*, 9347−9358.
(14) Fillinger, A.; Parkinson, B. A. *J. Electrochem. Soc.* **1999**, *146*, 4559−4564.
(15) Murakoshi, K.; Kano, G.; Wada, Y.; Yanagida, S.; Miyazaki, H.; Matsumoto, M.; Murasawa, S. *J. Electroanal. Chem.* **1995**, *396*, 27−34.
(16) Hara, K.; Sugihara, H.; Singh, L. P.; Islam, A.; Katoh, R.; Yanagida, M.; Sayama, K.; Murata, S.; Arakawa, H. *J. Photochem. Photobiol., A* **2001**, *145*, 117−122.
(17) Sauvé, G.; Cass, M. E.; Doig, S. J.; Lauermann, I.; Pomykal, K.; Lewis, N. S. *J. Phys. Chem. B* **2000**, *104*, 3488−3491.
(18) Strouse, G. F.; Schoonover, J. R.; Duesing, R.; Boyde, S.; Jones, W. E., Jr.; Meyer, T. J. *Inorg. Chem.* **1995**, *34*, 473−487.
(19) van Houten, J.; Watts, R. J. *J. Am. Chem. Soc.* **1976**, *98*, 4853−4858.
(20) Kuciauskas, D.; Freund, M. S.; Gray, H. B.; Winkler, J. R.; Lewis, N. S. *J. Phys. Chem. B* **2001**, *105*, 392−403.
(21) Kubelka, P. *J. Opt. Soc. Am.* **1948**, *38*, 448−457.
(22) Wesley, W.; Wendlandt, M.; Hecht, H. G. In *Reflectance Spectroscopy*; Interscience Publishers: New York, 1966; pp 55−65.
(23) Roundhill, D. M. In *Photochemistry and Photophysics of Metal Complexes*; Plenum Press: New York, 1994; Chapter 5.
(24) Andernon, P. A.; Strouse, G. F.; Treadway, J. A.; Keene, F. R.; Meyer, T. J. *Inorg. Chem.* **1994**, *33*, 3863−3864.
(25) Anderson, P. A.; Keene, R.; Meyer, T. J.; Moss, J. A.; Strouse, G. F.; Treadway, J. A. *J. Chem. Soc., Dalton Trans.* **2002**, 3820−3831.
(26) Caspar, J. V.; Westmoreland, T. D.; Allen, G. H.; Bradley, P. G.; Meyer, T. J.; Woodruff, W. H. *J. Am. Chem. Soc.* **1984**, *106*, 3492−3500.
(27) Argazzi, R.; Bignozzi, C. A.; Heimer, T. A.; Castellano, F. N.; Meyer, G. J. *Inorg. Chem.* **1994**, *33*, 5741−5749.
(28) Xie, P. H.; Hou, Y. J.; Zhang, B. W.; Cao, Y.; Wu, F.; Tian, W. J.; Shen, J. C. *J. Chem. Soc., Dalton Trans.* **1999**, 4217−4221.
(29) Nazeeruddin, M. K.; Kalyanasundaram, K. *Inorg. Chem.* **1989**, *28*, 4251−4259.
(30) Peterson, S. H.; Demas, J. N. *J. Am. Chem. Soc.* **1979**, *101*, 6571−6577.
(31) Timpson, C. J.; Bignozzi, C. A.; Sullivan, B. P.; Kober, E. M.; Meyer, T. J. *J. Phys. Chem.* **1996**, *100*, 2915−2925.
(32) Nazeeruddin, M. K.; Zakeeruddin, S. M.; Humphry-Baker, R.; Jirousek, M.; Liska, P.; Vlachopoulos, N.; Shklover, V.; Fischer, C. H.; Grätzel, M. *Inorg. Chem.* **1999**, *38*, 6298−6305.
(33) Toma, H. E.; Takasugi, M. S. *J. Solution Chem.* **1983**, *12*, 547−561.
(34) Toma, H. E.; Takasugi, M. S. *J. Solution Chem.* **1989**, *18*, 575−583.
(35) Schilt, A. A. *J. Am. Chem. Soc.* **1960**, *82*, 3000−3005.
(36) Duffy, N. W.; Dobson, K. D.; Gordon, K. C.; Robinson, B. H.; McQuillan, A. J. *Chem. Phys. Lett.* **1997**, *266*, 451−455.
(37) Deacon, G. B.; Phillips, R. J. *Coord. Chem. Rev.* **1980**, *33*, 227−250.
(38) Mehrotra, R. C.; Bohra, R. *Metal Carboxylates*; Academic Press: New York, 1983.
(39) Katz, J., California Institute of Technology, 2004. Personal communication.
(40) Shklover, V.; Ovchinnikov, Y. E.; Braginsky, L. S.; Zakeeruddin, S. M.; Grätzel, M. *Chem. Mater.* **1998**, *10*, 2533−2541.